Intensity autocorrelation measurements of frequency combs in the terahertz range

Ileana-Cristina Benea-Chelmus,* Markus Rösch, Giacomo Scalari, Mattias Beck, and Jérôme Faist†
ETH Zurich, Institute of Quantum Electronics, Auguste-Piccard-Hof 1, Zurich 8093, Switzerland
(Received 10 July 2017; published 12 September 2017)

We report on direct measurements of the emission character of quantum cascade laser based frequency combs, using intensity autocorrelation. Our implementation is based on fast electro-optic sampling, with a detection spectral bandwidth matching the emission bandwidth of the comb laser, around 2.5 THz. We find the output of these frequency combs to be continuous even in the locked regime, but accompanied by a strong intensity modulation. Moreover, with our record temporal resolution of only few hundreds of femtoseconds, we can resolve correlated intensity modulation occurring on time scales as short as the gain recovery time, about 4 ps. By direct comparison with pulsed terahertz light originating from a photoconductive emitter, we demonstrate the peculiar emission pattern of these lasers. The measurement technique is self-referenced and ultrafast, and requires no reconstruction. It will be of significant importance in future measurements of ultrashort pulses from quantum cascade lasers.

DOI: 10.1103/PhysRevA.96.033821

I. INTRODUCTION

Frequency combs [1] are sources of electromagnetic radiation, which have phase-stable frequency components equidistantly spaced in frequency domain. This property qualifies them as highly precise spectral rulers, and has promoted their use for high-precision metrology [1], for telecommunication [2], as well as for high-resolution spectroscopy [3–5]. The traditional way to realize frequency combs is from mode-locked lasers [6], which in time domain represent a Fourier-limited train of pulses [7]. Nowadays, numerous alternative means have been demonstrated, with notable results based on high harmonic generation in the extreme ultraviolet and soft x rays [8,9], phase-locked lasers in the optical and near-infrared (NIR) domain [10], Kerr effect in microresonators for the NIR [11], and mid-infrared (MIR) [12,13].

In the MIR [14] and the terahertz (THz) region of the electromagnetic spectrum [15,16], the most compact and efficient frequency combs are from electrically injected quantum cascade lasers (QCL) [17]. They have been shown to produce high-power, high-bandwidth frequency combs, with Shawlow-Townes limited spectral purity [18,19]. The coherence of the comb components is generated by four-wave mixing [20], a $\chi^{(3)}$ nonlinear process [21], where, in the frequency domain, the nonlinear mixing of equidistant frequency components is parametrically enhanced by energy conservation. An important alternative to QCL combs in the THz are from optically pumped photoconductive elements which can produce high-field-pulsed radiation upon optical rectification of a femtosecond pulse [22].

Alongside with the frequency precision, the time-domain emission profile of frequency combs is of major importance in experiments. For example, oscillating electric fields exceeding MV/m from Fourier-limited THz pulses are utilized for impact ionization [23], high harmonic generation [24], whereas continuous-wave emission is preferred for nondestructive spectroscopic applications.

In the case of QCL frequency combs, the upper state lifetime of intersubband transitions is short in comparison to the cavity round-trip time [25]. This affects the temporal dynamics of QCL combs. Theoretical work suggests that passive pulse formation is not possible in QCL combs even in the case of zero dispersion, and that their output resembles the one of continuous-wave lasers [20,26]. Also, experimentally, the only successful approaches to generate pulses from QCLs are indirect, based on injection seeding the active medium with picosecond short pulses from a photoconductive antenna [27,28], or on active mode locking [29,30]. In these particular cases, the emitted terahertz light is phase locked to a reference femtosecond oscillator, and its output profile could be measured by coherent electro-optic sampling [31,32]. For the case of free-running QC combs, in the absence of pulse emission, the method of choice of characterization has long been beat-note analysis, a purely frequency-domain technique. The only available technique to retrieve the complete time-domain information of QCL combs is shifted wave interference, that requires both a tunable local oscillator and subsequent waveform reconstruction [33], which renders the technique very evolved.

At frequencies other than the THz range, as for example in the NIR, the time-domain properties of combs are routinely assessed by intensity autocorrelation, a simple and fast time-domain technique based on second harmonic generation of the light wave with a delayed replica using a $\chi^{(2)}$ medium [34,35]. Recently, we reported on a technique to measure electric field and intensity correlations at THz frequencies by electro-optic sampling with a very short temporal resolution of 146 fs [36]. This technique is optimally suited for the investigation of long- and short-scale correlations of QCL based frequency combs since the temporal resolution of this technique is even shorter than one cycle of oscillation. It can therefore resolve correlations which are intracycle (shorter than 400 fs), at time scales of the gain recovery time, typically only a few picoseconds [37], and cavity round-trip times, few tens of picoseconds. This is the main advantage of this technique.

*ileanab@ethz.ch
†jerome.faist@phys.ethz.ch

In this work, we exploit this autocorrelation to get insight into the output dynamics of THz QCL frequency combs. We provide a short mathematical support to emphasize the potential of the technique when applied to frequency combs. Several devices have been tested and show qualitatively similar behavior, and in this paper we limit the results section to a representative laser device. The laser is operating as a low-noise frequency comb at low-input current where it spans the spectral range from 2.2–2.8 THz, and in the dispersed regime at high-input current, where the emission is more broadband, reaching a maximum from 1.6–3.3 THz. The detailed performance and spectral characteristics of the investigated device have been reported in Refs. [15,17]. We compare the results with the emission profile of a pulsed frequency comb in the terahertz based on optical rectification in a photoconductive antenna.

II. FAST CORRELATIONS OF FREQUENCY COMBS

A schematics of the autocorrelation measurement method is shown in Fig. 1(a). The operation principle relies on the nonlinear interaction between the THz wave and an ultrashort near-infrared (NIR) probing pulse [36] inside a nonlinear crystal which exhibits a $\chi^{(2)}$ nonlinearity. The terahertz wave induces a change in the refractive index of the crystal, which is linearly dependent on the electric field of the THz wave (Pockels). This changes the polarization of the femtosecond short probing pulse, which is finally measured using balanced detectors. Two mutually delayed (τ) ultrashort near-infrared (NIR) probing pulses [36] are employed to measure field and intensity correlations. They are sampling the electric field of the THz wave at two distinct points in time (t), with the associated measurement results denoted in the following $\mathcal{E}(t)$ and $\mathcal{E}(t+\tau)$. From these two measurements we compute the normalized autocorrelation functions, denoted $g^{(1)}(\tau)$ and $g^{(2)}(\tau)$ and defined as follows:

$$g^{(1)}(\tau) = \frac{\langle \mathcal{E}_{\mathrm{THz}}(t)\mathcal{E}_{\mathrm{THz}}(t+\tau)\rangle_t}{\sqrt{\langle \mathcal{E}_{\mathrm{THz}}(t)\mathcal{E}_{\mathrm{THz}}(t)\rangle_t \langle \mathcal{E}_{\mathrm{THz}}(t+\tau)\mathcal{E}_{\mathrm{THz}}(t+\tau)\rangle_t}}, \tag{1}$$

$$g^{(2)}(\tau) = \frac{\left\langle \mathcal{E}^2_{\mathrm{THz}}(t)\mathcal{E}^2_{\mathrm{THz}}(t+\tau)\right\rangle_t}{\left\langle \mathcal{E}^2_{\mathrm{THz}}(t)\right\rangle_t \left\langle \mathcal{E}^2_{\mathrm{THz}}(t+\tau)\right\rangle_t}. \tag{2}$$

$\langle \ldots \rangle_t$ represent averages over time and $G^{(1)}(\tau)$ and $G^{(2)}(\tau)$ are their not-normalized counterparts.

A detailed description of the setup and measurement algorithm can be found in [36]. We match the emission bandwidth of the laser with the detection bandwidth of the nonlinear effect by choosing a 3-mm-long zinc telluride [ZnTe, (110)] crystal as detection medium. To evidentiate this fact, we show in Fig. 1(b) in full line the computed coherence length in this configuration, using $l_c = \frac{\pi c}{2\pi f_{\mathrm{THz}} |n_{g,\mathrm{opt}} - n_{\mathrm{ph,THz}}|}$, where we marked the spectral regions where the laser is emitting in the comb (2.2–2.8 THz) and dispersed regime (1.6–3.3 THz). In addition, the absorption inside the detection crystal is moderate at these frequencies, as shown with the dashed line.

Each of the autocorrelation functions will be utilized to infer complementary information about the operation mode of the comb lasers. If we define the emission of our frequency comb as a discrete Fourier sum of equidistant frequency components with independent, but fixed, amplitudes E_i and phases ϕ_i,

$$\mathcal{E}_{\mathrm{THz}}(t) = \sum_i E_i \cos(\omega_i t + \phi_i) \tag{3}$$

with no restriction on the amplitudes nor on the phases of the spectral components, we find that the first-order autocorrelation function can be simplified to

$$g^{(1)}(\tau) = \frac{\sum_i E_i^2 \cos(\omega_i \tau)}{\sum_i E_i^2}. \tag{4}$$

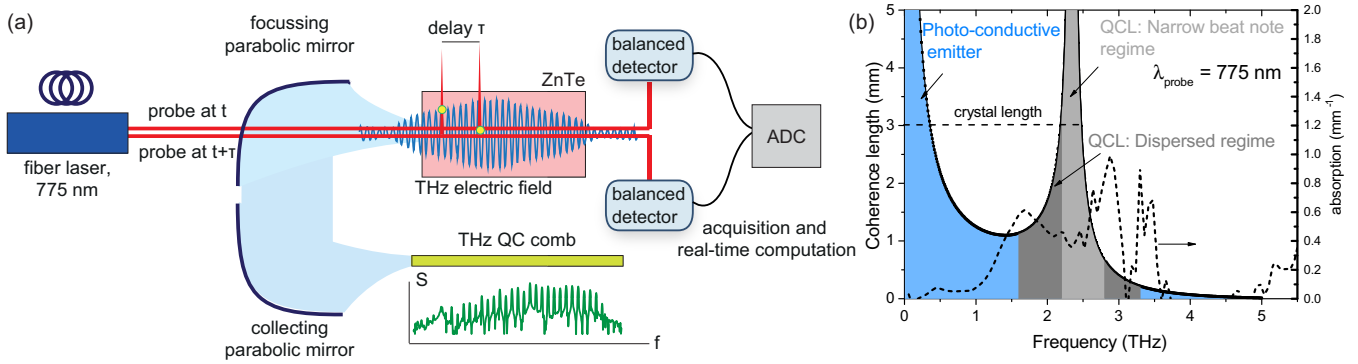

FIG. 1. Measurement setup and detector bandwidth. (a) Time-domain correlation setup based on two-probe electro-optic sampling. The two probes sample the THz radiation of a QCL based frequency comb at two mutually delayed points in time. The probe pulse length is 146 fs. A fast acquisition module records the two sampled values and a further real-time routine computes from here the instantaneous intensity, and the two-point electric field and intensity product. When averaged over time and normalized, this gives the autocorrelation functions $g^{(1)}(\tau)$ and $g^{(2)}(\tau)$. (b) Calculated coherence length of the THz detection in a (110)-oriented ZnTe, and a probe center wavelength of 775 nm (full line), together with measured absorption in ZnTe at 300 K (dashed line). The detectivity is matched to the laser comb emission, which is marked for when the investigated laser is operating in a narrow beat-note regime, 2.2–2.8 THz (light gray), and dispersed regime, 1.6–3.3 THz (dark gray).

This result shows clearly that any fixed phase relation that exists between the modes is irrelevant for $g^{(1)}(\tau)$. Therefore, a measurement of $g^{(1)}(\tau)$ is insufficient to determine the type of modulation present in the laser since both amplitude- and frequency-modulated lasers require a strict phase distribution among the modes, which is exhaustively explained here [38]. Also obvious, the first-order autocorrelation function $g^{(1)}(\tau)$ gives the power spectrum of emission, through the Wiener-Khinchine theorem [39]. We need higher-order correlation functions to determine the characteristics of the emission pattern of THz QCL combs.

The second-order autocorrelation function $g^{(2)}(\tau)$, found in Eq. (2), can be rewritten in intensity terms, with $\mathcal{I} = c\epsilon_0\epsilon_r\mathcal{E}^2$. The quantity $g^{(2)}(\tau)$ is 1 when the intensities $\mathcal{I}(t)$ and $\mathcal{I}(t+\tau)$ are fully uncorrelated and can be factorized:

$$g^{(2)}(\tau) = \frac{\langle \mathcal{I}(t)\mathcal{I}(t+\tau)\rangle_t}{\langle \mathcal{I}(t)\rangle_t \langle \mathcal{I}(t+\tau)\rangle_t} = \frac{\langle \mathcal{I}(t)\rangle_t \langle \mathcal{I}(t+\tau)\rangle_t}{\langle \mathcal{I}(t)\rangle_t \langle \mathcal{I}(t+\tau)\rangle_t} = 1. \quad (5)$$

More importantly for our analysis about the output profile of comb lasers, for classical radiation, the value of $g^{(2)}(\tau = 0)$ gives particular insight into the intensity modulation depth since it can be rewritten as

$$g^{(2)}(\tau = 0) = \frac{\langle \mathcal{I}(t)^2\rangle_t}{\langle \mathcal{I}(t)\rangle_t^2} = 1 + \frac{\mathrm{Var}[\mathcal{I}(t)]}{\langle \mathcal{I}(t)\rangle_t^2}, \quad (6)$$

where $\mathrm{Var}[\mathcal{I}(t)]$ represents the variance of the intensity. From here, we define the amplitude modulation depth in the following way:

$$\frac{\sqrt{\mathrm{Var}[\mathcal{I}(t)]}}{\langle \mathcal{I}(t)\rangle_t} = \sqrt{g^{(2)}(\tau = 0) - 1}. \quad (7)$$

At time delays other than $\tau = 0$, the non-normalized second-order autocorrelation $G^{(2)}(\tau)$ is

$$\begin{aligned} G^{(2)}(\tau) &= \left\langle \mathcal{E}^2_{\mathrm{THz}}(t)\mathcal{E}^2_{\mathrm{THz}}(t+\tau)\right\rangle_t \\ &= \frac{1}{8}\sum_{i,j,ii,jj} E_i E_{ii} E_j E_{jj} \\ &\quad \times \{2\langle \cos[(\omega_i + \omega_j - \omega_{ii} - \omega_{jj})t + (\omega_j - \omega_{jj})\tau \\ &\quad + \phi_i + \phi_j - \phi_{ii} - \phi_{jj}]\rangle_t \\ &\quad + \langle \cos[(\omega_i + \omega_j - \omega_{ii} - \omega_{jj})t + (\omega_j + \omega_i)\tau \\ &\quad + \phi_i + \phi_j - \phi_{ii} - \phi_{jj}]\rangle_t\}. \end{aligned} \quad (8)$$

Both terms are nonzero only if $\omega_i + \omega_j = \omega_{ii} + \omega_{jj}$ and $\langle \phi_i + \phi_j - \phi_{ii} - \phi_{jj}\rangle =$ fixed, so precisely in the case of frequency combs, which fulfill these conditions. $g^{(2)}(\tau)$ can be retrieved from $G^{(2)}(\tau)$ by normalization with $\langle \mathcal{E}^2_{\mathrm{THz}}(t)\rangle_t \langle \mathcal{E}^2_{\mathrm{THz}}(t)\rangle_t = \frac{1}{4}(\sum_i E_i^2)^2$.

For a laser, where all modes are mutually free running [i.e., $\langle \phi_i + \phi_j - \phi_{ii} - \phi_{jj}\rangle \neq$ fixed unless $i = ii = j = jj$ or $(i = ii) \neq (j = jj)$ or $(i = jj) \neq (j = ii)$] we find

$$\begin{aligned} \left\langle \mathcal{E}^2_{\mathrm{THz}}(t)\mathcal{E}^2_{\mathrm{THz}}(t+\tau)\right\rangle_t &= \frac{1}{8}\sum_i E_i^4[2 + \cos(2\omega_i\tau)] + \frac{1}{8}\sum_i \\ &\quad \times \sum_{j,j\neq i} 2E_i^2E_j^2\{1 + \cos[(\omega_j - \omega_i)\tau] \\ &\quad + \cos[(\omega_j + \omega_i)\tau]\}. \end{aligned} \quad (9)$$

In particular, we find that the subcycle value of $g^{(2)}(\tau = 0)$ for fully unlocked sources is

$$g^{(2)}(\tau = 0) = \frac{3}{2}\left[2 - \frac{\sum_i E_i^4}{\left(\sum_i E_i^2\right)^2}\right] < 3. \quad (10)$$

In addition to this, the few-cycle running average, over time scales that are longer than the characteristic oscillation frequency of the intensity autocorrelation function {fast oscillating terms $\langle \cos(2\omega_i\tau)\rangle = 0$, $\langle \cos[(\omega_j + \omega_i)\tau]\rangle = 0$ and slow oscillating terms $\langle \cos[(\omega_j - \omega_i)\tau]\rangle = 1$} yields

$$g^{(2)}(\tau = 0) = \frac{\sum_i E_i^4 + 2\sum_i \sum_{j,j\neq i} E_i^2E_j^2}{\left(\sum_i E_i^2\right)^2} < 2 \text{ and } \geqslant 1. \quad (11)$$

The upper bound is reached in the limit of many unlocked modes, thus, thermal radiation, and the lower bound is a single-mode laser (see Ref. [36] for examples).

At the opposite extreme, for the case of fully locked sources, the subcycle value of $g^{(2)}(\tau = 0)$ is

$$g^{(2)}(\tau{=}0){=}\frac{3}{2}\frac{\sum_{i,j,ii,jj} E_i E_{ii} E_j E_{jj} \cos(\phi_i{+}\phi_j{-}\phi_{ii}{-}\phi_{jj})}{\left(\sum_i E_i^2\right)^2}, \quad (12)$$

where the sum runs over any combination that fulfills the condition $\omega_i + \omega_j = \omega_{ii} + \omega_{jj}$. From this equation, we find clearly that $g^{(2)}(\tau = 0)$ depends on the phases of the locked modes present in the laser in a nontrivial way. Moreover, $g^{(2)}(\tau = 0)$ reaches the maximum value for given mode distribution for the case where $\phi_i + \phi_j - \phi_{ii} - \phi_{jj} = 0$ for all modes, that is, for the case of Fourier-limited pulses, where $\phi_i = \phi_j = \phi_{ii} = \phi_{jj}$. This evidentiates the generic initial statement that emission with a high modulation depth has a high $g^{(2)}(\tau = 0)$.

In conclusion, the measurement of $g^{(2)}(\tau)$ is sensitive to many effects which determine the comb operation of a device: It depends on the mutual phase coherence of the lasing modes, and is maximized for emission of Fourier-limited pulses; it is also sensitive to incoherent radiation, such as thermal drifts; and it gives insight into the modulation type present in the laser.

Moreover, to disentangle the incoherent from the coherent phase-stable effects, one has to look at time delays other than $\tau = 0$. In particular, incoherent radiation has a stable output power, but intensity correlations occur only on short time scales, that is, only around $\tau = 0$. Quite on the opposite, frequency combs are mutually coherent and have an almost perfectly repetitive emission profile at the round trip and, therefore, intensity correlations persist around $\tau = 0$ as well as multiple of the repetition rate $\tau = nT_{\mathrm{rep}}$. In the results section, we exemplify precisely these features by applying $g^{(2)}(\tau)$ measurements on two types of frequency combs in the THz region.

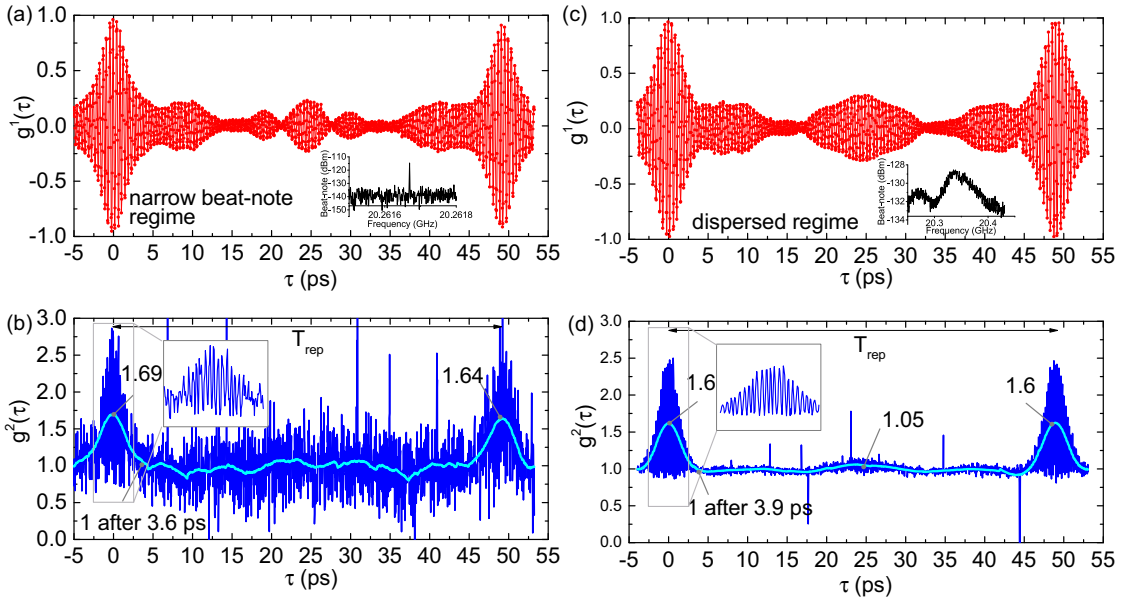

FIG. 2. First- and second-order autocorrelation measurements of a 2-mm-long THz laser comb operating in the narrow beat-note regime [(a), (b)] and the dispersed regime [(c), (d)]. Insets show a zoom-in into the $g^{(2)}(\tau)$ around $\tau = 0$ to evidentiate the subcycle intensity resolution of the technique. (a) $g^{(1)}(\tau)$ measurement of laser emission in the narrow beat-note regime, at 906 mA and $T = 23$ K. Inset: beat note at 900 mA. (b) $g^{(2)}(\tau)$ in the narrow beat-note regime. For long time delays, the intensity decays to 1, and therefore uncorrelated but continuous-wave-like. (c) $g^{(1)}(\tau)$ measurement of laser emission in the dispersed regime, at 1010 mA and $T = 23$ K. Inset: beat note at 1000 mA. (d) $g^{(2)}(\tau)$ measurement of laser emission in the dispersed regime. For long time delays, the intensity becomes uncorrelated, and decays again to a value of 1. Light (blue) lines represent few-cycle average of the $g^{(2)}(\tau)$, to filter the subcycle resolution of the intensity autocorrelation (window averaging 5 ps).

III. CURRENT-DEPENDENT CORRELATIONS OF QCL COMBS

We investigate now the dynamics of the QCL based laser comb when operated in the narrow beat-note regime, at 906 mA, and dispersed regime, at 1010 mA. The QCL based frequency comb was operated in quasi-continuous-wave (cw) mode with a very slow modulation frequency of 2.5 kHz and 50% duty cycle. The cw output power of the laser at these two operating points was 1.05 and 2.96 mW, respectively, as measured with a Thomas-Keiting power meter.

The laser is 2 mm long and 150 μm wide, corresponding to a repetition rate of 20.3 GHz. The cavity of the laser is constituted of a double-metal cavity for good temperature and dispersion performance and cryocooled to 23 K [15].

The measured first- and second-order autocorrelation functions are reported in Fig. 2 as a function of time delay τ. The electric field interferogram $g^{(1)}(\tau)$ is reported at operation points in the narrow beat note, at 900 mA [Fig. 2(a)] and the dispersed regime, at 1010 mA [Fig. 2(c)], and exhibits a repetition period of 49.5 ps, corresponding to the expected repetition rate of 20.3 GHz. At $\tau = 0$, $g^{(1)}(\tau) = 0.98$ at both operating points, approximating well the theoretically expected value of 1. The beat notes of the comb lasers are reported in the inset when operated in continuous wave, at 900 and 1000 mA, respectively.

The intensity autocorrelation $g^{(2)}(\tau)$ is reported in Figs. 2(b) and 2(d). The intensity autocorrelation is oscillatory due to the subcycle temporal resolution, with a characteristic frequency of double the emission frequency, as can be seen in the insets. Therefore, correlated intensity fluctuations occurring at subcycle time scales could be measured. To retrieve long-range behavior, we perform a running average filtering (window width of 5 ps) to filter out these oscillations, and establish the few-cycle regime which carries information about the intensity correlations of the emission. The result is reported by the cyan colored (light) line. In the comb regime, the intensity autocorrelation function takes a few-cycle average value of 1.69. These modes lead therefore to persistent intensity correlations. Using the above-developed arguments, this suggests that $\frac{\sqrt{\mathrm{Var}[I(t)]}}{\langle I(t)\rangle_t} = \sqrt{0.69} = 0.83$ and, consequently, that the intensity modulation depth as defined previously is roughly 83%. In addition, $g^{(2)}(\tau)$ decreases to a value of 1 after roughly 3.6 ps, showing that correlated intensity modulations take place on time scales as short as 3.9 ps. This time scale is governed by the gain recovery time, after which population inversion is reestablished. This incredibly short time, as compared to the repetition rate, of the laser is at the origin that passive QCLs do not emit pulses.

At longer time scales, the intensity autocorrelation function is roughly constant to 1, which suggests the peculiar continuous-wave-like output. Clearly, in this case, even if the field is coherent, suggested by the interference fringes, the intensity itself has no predetermined correlations. In addition, we clearly find that intensity correlations are reestablished after a full round-trip time. At $\tau = T_{\mathrm{rep}}$, $g^{(2)}(T_{\mathrm{rep}}) = 1.64$, lower than $g^{(2)}(0)$. This fact might suggest a drift in the laser.

In the dispersed regime, $g^{(2)}(\tau)$ decreases to 1 after 3.9 ps, and decays from a value of 1.6 at $\tau = 0$. This value is slightly lower than the one in the comb regime, and could suggest that in this case, the emission is less pulsed. Similarly, this

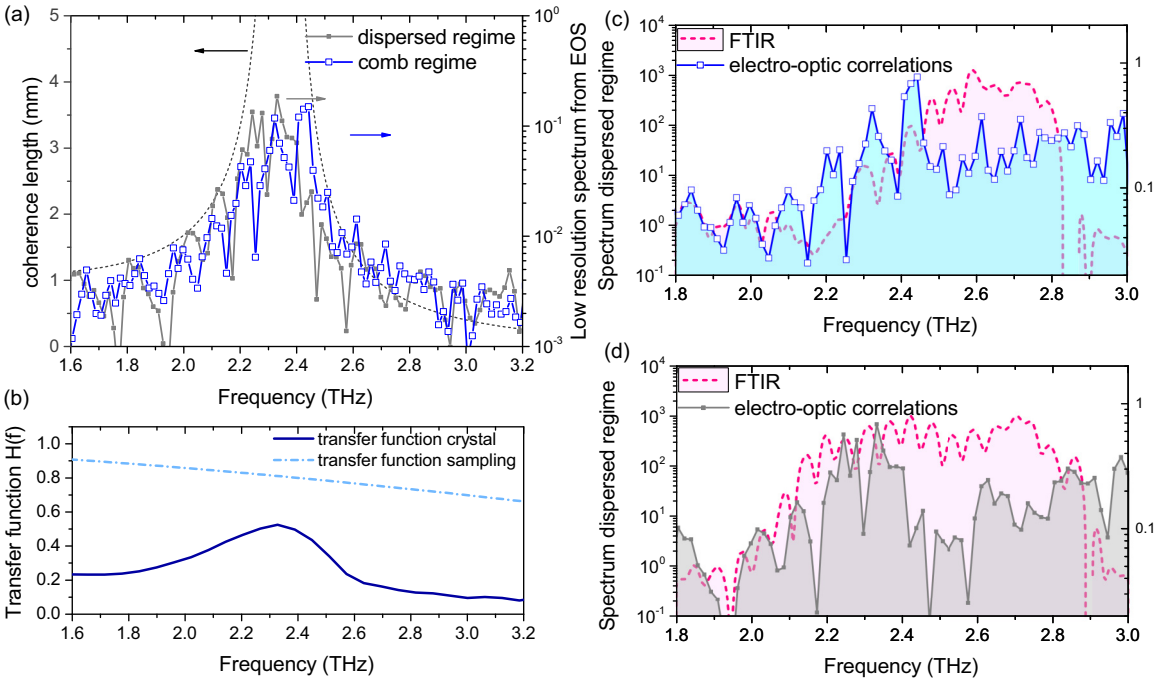

FIG. 3. Spectral analysis of the QCL based frequency comb when operated in the narrow beat-note and dispersed regime, using electro-optic correlations. (a) Low-resolution amplitude spectra from the Fourier transformation of $g^{(1)}(\tau)$ [gray (full squares) and blue (empty squares)], shown together with coherence length computations for ZnTe and a center probe wavelength of 775 nm. (b) Transfer function of the detection based on ZnTe under these conditions, where absorption at room temperature has been taken into account (blue full line) shown together with the transfer function of electro-optic sampling (blue dotted-dashed line). (c) Emitted THz power spectrum from electro-optic sampling (using the transfer function of the crystal in (b)] when the laser is operated in comb regime compared to a low-resolution FTIR measurement. (d) Emitted THz power spectrum from electro-optic sampling (using the transfer function in (b)] when the laser is operated in the dispersed regime compared to a low-resolution FTIR measurement [15,17].

suggests that $\frac{\sqrt{\mathrm{Var}[I(t)]}}{\langle I(t)\rangle_t} = \sqrt{0.6} = 0.77$ and, consequently, that the intensity modulation depth is roughly 77%. In addition, this intensity modulation takes place on similar time scales, 3.9 ps. Also in this case, the intensity correlations are established after a full repetition rate, and in this case $g^{(2)}(0) = g^{(2)}(T_{\mathrm{rep}}) = 1.6$, even though this regime exhibits a broad beat-note regime. We give a possible explanation to this effect in the next section, where the spectral characteristics are investigated. Additionally, intensity correlations occur also at half the round-trip time, with a $g^{(2)}(\frac{T_{\mathrm{rep}}}{2}) = 1.05$.

IV. BANDWIDTH OF DETECTION

Our technique is spectrally resolving. The direct measurement of electric field autocorrelation $g^{(1)}(\tau)$ has been Fourier transformed to retrieve the low-resolution spectrum of the THz source. The results are reported in Fig. 3(a), for the comb and dispersed regime, together with the coherence length of ZnTe, which is obviously spectrally limiting and not flat. Therefore, the measured signal E_{detected} is a convolution of the real laser emission $E_{\mathrm{emitted}}(f)$ and the detection sensitivity of the ZnTe crystal:

$$E_{\mathrm{detected}}(f) = E_{\mathrm{emitted}} H(f).$$

The transfer function of a 3-mm-long ZnTe crystal is reported in Fig. 3(b), as measured with standard time-domain spectroscopy from comparison with a very thin crystal (200 μm), where a flat response was assumed. It includes both the effects of coherence and of THz absorption in ZnTe, which is particularly strong in this region due to phonon resonances. The transfer function is further used to retrieve the power spectrum of the THz source:

$$S_{xx,\mathrm{detected}}(f) = S_{xx,\mathrm{emitted}} H^2(f).$$

Finally, we compare the low-resolution spectra as obtained by electro-optic sampling with low-resolution Fourier transform infrared spectroscopy (FTIR) setup in Figs. 3(c) and 3(d). We find that, in contrast to the spectrum as measured by the FTIR, the nonflat sensitivity of electro-optic detection leads to a shaping of the spectrum especially at high frequencies, which can not be fully retrieved from noise even if accounted for. This sensitivity profile has its origin both in the coherence length of the crystal and in the cutoff at Nyquist limit due to slightly longer femtosecond pulses (corresponding to a Nyquist limit of lower than 3.3 THz), both shown in Fig. 3(b). The beat note on the contrary is composed by all frequency components in the laser. This might explain why the measurements of $g^{(2)}(\tau)$ are so similar for the two regimes, even though the beat notes are clearly different. The spectral region probed by electro-optic correlations might in fact be a locked comb. To probe this hypothesis, one would have to spectrally shift the detection window of ZnTe throughout the full emission spectrum of the QCL. This is in principle possible by tuning the wavelength of the probe, as shown in Ref. [40], but is not possible in our setup now.

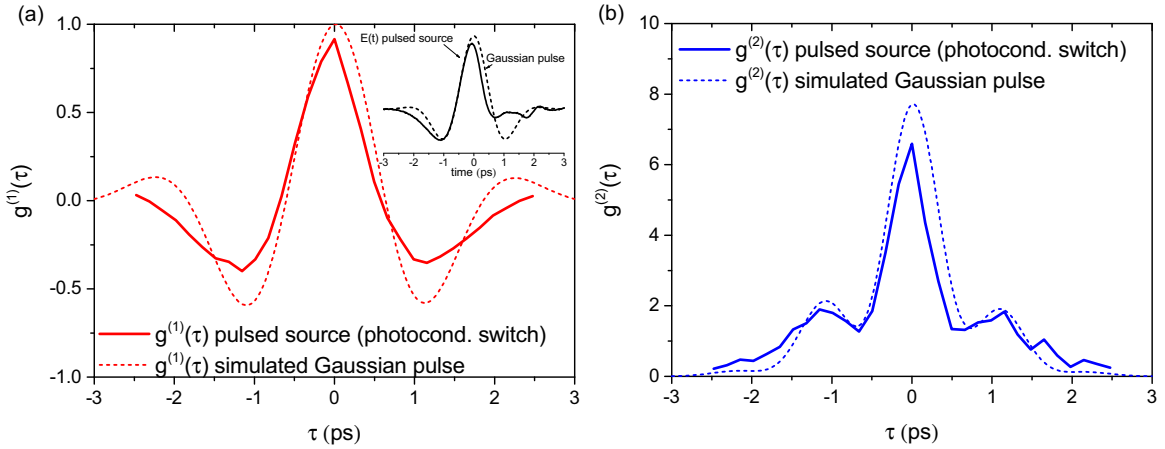

FIG. 4. Results of first- and second-order autocorrelation of a pulsed THz comb based on optical rectification in a photoconductive emitter, using the same correlation technique. (a) $g^{(1)}(\tau)$ of the THz pulse with an electric field profile as shown in the inset. We compare the measurement to a simulated pulse with Gaussian spectrum and find qualitatively good agreement. (b) $g^{(2)}(\tau)$ of the pulsed radiation, normalized to the average intensity within a time window of 13 ps. Characteristic to pulsed radiation is the decay of the intensity autocorrelation function to a value of 0, which is a clear indicator for the pulsed emission and the value at zero path delay of 6.59.

V. INTENSITY CORRELATIONS OF PULSED EMISSION FROM PCAS

We have demonstrated so far that THz quantum cascade laser based frequency combs have a continuous emission with strong intensity modulation. These peculiar properties remain in big contrast to conventional frequency combs, where the emission is typically pulsed. Such pulsed sources have been realized in the terahertz domain by optical rectification of femtosecond pulses in $\chi^{(2)}$ media.

We measure the field and intensity autocorrelation functions of the pulsed THz radiation emitted by a photoconductive emitter, by optical rectification of femtosecond laser pulses at 775 nm. The results are shown in Fig. 4, together with analytical simulations, which assume a simplified scenario of a THz pulse with Gaussian spectrum, no dispersion, and a spectral width roughly coinciding with the one of the photoconductive emitter. This simplified example is instructive enough to reproduce the main characteristics.

The electric field of the emission has been measured by coherent electro-optic sampling and is shown in the inset in Fig. 4(a). The autocorrelation functions have been measured by the two-beam technique utilized also for the laser comb. They are measured for a time delay as long as the main temporal extent of the pulse, roughly 6 ps. The first-order autocorrelation function $g^{(1)}(\tau)$ has an almost perfectly symmetric shape around $\tau = 0$, as expected. The slight asymmetry has its origin in small imperfections in the optical setup for positive and negative time delays, such as beam walk. The most instructive characteristic is, however, in the shape and peak value of the second-order autocorrelation function $g^{(2)}(\tau)$. It decays to a value of 0 after roughly 2.5 ps, which suggests the pulsed character of the emission. This is in strong contrast to the emission of quantum cascade laser combs, where the continuous-wave-like output results in a $g^{(2)}(\tau)$ which decays to 1. Moreover, $g^{(2)}(0)$ at zero path delay is 6.59, when normalized to the average intensity in a time window of 13 ps. Among all our measurements, this value is maximized for pulsed emission, as we expected from the brief mathematical derivation. For completeness, these results can be also compared to measurements of single-mode lasers, where $g^{(2)}(0)$ is 1, and therefore the intensity modulation depth is 0%. Such results can be found in [36].

VI. DISCUSSION AND CONCLUSION

We have demonstrated direct measurement of intensity correlations of a quantum cascade laser based frequency comb, and compared these results to mode-locked THz combs generated by optical rectification in a photoconductive emitter. We found that the laser emission is characterized by a strong amplitude modulation of 83% in the comb regime and 77% in the dispersed regime. The continuous-wave-like output of the laser becomes visible through the intensity autocorrelation function which decays to 1, in contrast to pulsed sources where it decays to 0.

For this purpose, we utilized a technique which has a temporal resolution of 150 fs, only a fraction of one period of light, and is in addition sensitive to any incoherent components [36] in the light wave through its self-referenced character. With such short temporal resolution we could determine that intensity correlations persist over time scales as short as the gain recovery time of the laser, a few picoseconds.

Having the possibility to quickly assess the emission profile of free-running lasers in the terahertz frequency range is an important technological milestone. In future, quantum cascade lasers based combs, which are inherently frequency modulated, could be transformed into amplitude-modulated combs by use of an external spatial light modulator to fulfill the zero phase condition for Fourier-limited pulses. Our technique will be here of big importance to minimize in real time the temporal extent of the pulse by controlling $g^{(2)}(\tau = 0)$ and provide feedback to the actuating phase

plate. Also, harmonic states in QCLs might become a source of pulsed radiation [38] with beat tones up to over 100 GHz, making their analysis with beat-note spectroscopy very difficult. Here again, autocorrelators will be of high importance.

More generally, the technique is perfectly suited to measure fluctuations faster than one oscillation period, thus subcycle. We are convinced that many more fundamental experiments can be envisaged.

ACKNOWLEDGMENTS

We acknowledge the insightful comments of C. Bonzon on the data and his expertise with cryogenic measurements. We also acknowledge the work of the mechanical workshop at ETHZ. The authors would like to acknowledge funding from the European Research Council (Advanced Grant, Quantum Metamaterials in the Ultra Strong Coupling Regime). The sample growth and processing took place in the clean room facility of ETHZ, FIRST center.

[1] T. Udem, J. Reichert, R. Holzwarth, and T. W. Hänsch, Absolute Optical Frequency Measurement of the Cesium D 1 Line with a Mode-Locked Laser, Phys. Rev. Lett. **82**, 3568 (1999).

[2] J. Pfeifle, V. Brasch, M. Lauermann, Y. Yu, D. Wegner, T. Herr, K. Hartinger, P. Schindler, J. Li, D. Hillerkuss, R. Schmogrow, C. Weimann, R. Holzwarth, W. Freude, J. Leuthold, T. J. Kippenberg, and C. Koos, Coherent terabit communications with microresonator Kerr frequency combs, Nat. Photonics **8**, 375 (2014).

[3] R. Holzwarth, T. Udem, T. Hansch, J. Knight, W. Wadsworth, and P. Russell, Optical Frequency Synthesizer for Precision Spectroscopy, Phys. Rev. Lett. **85**, 2264 (2000).

[4] G. Villares, A. Hugi, S. Blaser, and J. Faist, Dual-comb spectroscopy based on quantum-cascade-laser frequency combs, Nat. Commun. **5**, 5192 (2014).

[5] M. Rösch, G. Scalari, G. Villares, L. Bosco, M. Beck, and J. Faist, On-chip, self-detected terahertz dual-comb source, Appl. Phys. Lett. **108**, 171104 (2016).

[6] T. Udem, R. Holzwarth, and T. Hansch, Optical frequency metrology, Nature (London) **416**, 233 (2002).

[7] S. T. Cundiff and J. Ye, Colloquium: Femtosecond optical frequency combs, Rev. Mod. Phys. **75**, 325 (2003).

[8] M. Chini, K. Zhao, and Z. Chang, The generation, characterization and applications of broadband isolated attosecond pulses, Nat. Photonics **8**, 178 (2014).

[9] C. Altucci, J. W. G. Tisch, and R. Velotta, Single attosecond light pulses from multi-cycle laser sources, J. Mod. Opt. **58**, 1585 (2011).

[10] D. Jones, S. Diddams, J. Ranka, A. Stentz, R. Windeler, J. Hall, and S. Cundiff, Carrier-envelope phase control of femtosecond mode-locked lasers and direct optical frequency synthesis, Science **288**, 635 (2000).

[11] P. Del'Haye, A. Schliesser, O. Arcizet, T. Wilken, R. Holzwarth, and T. J. Kippenberg, Optical frequency comb generation from a monolithic microresonator, Nature (London) **450**, 1214 (2007).

[12] A. G. Griffith, R. K. W. Lau, J. Cardenas, Y. Okawachi, A. Mohanty, R. Fain, Y. H. D. Lee, M. Yu, C. T. Phare, C. B. Poitras, A. L. Gaeta, and M. Lipson, Silicon-chip mid-infrared frequency comb generation, Nat. Commun. **6**, 6299 (2015).

[13] C. Y. Wang, T. Herr, P. Del'haye, A. Schliesser, J. Hofer, R. Holzwarth, T. W. Hänsch, N. Picqué, and T. J. Kippenberg, Mid-infrared optical frequency combs at 2.5 mum based on crystalline microresonators, Nat. Commun. **4**, 1345 (2013).

[14] A. Hugi, G. Villares, S. Blaser, H. C. Liu, and J. Faist, Mid-infrared frequency comb based on a quantum cascade laser, Nature (London) **492**, 229 (2012).

[15] M. Rösch, G. Scalari, M. Beck, and J. Faist, Octave-spanning semiconductor laser, Nat. Photonics **9**, 42 (2015).

[16] D. Burghoff, T.-Y. Kao, N. Han, C. W. I. Chan, X. Cai, Y. Yang, D. J. Hayton, J.-R. Gao, J. L. Reno, and Q. Hu, Terahertz laser frequency combs, Nat. Photonics **8**, 462 (2014).

[17] J. Faist, G. Villares, G. Scalari, M. Rösch, C. Bonzon, A. Hugi, and M. Beck, Quantum cascade laser frequency combs, Nanophotonics **5**, 272 (2016).

[18] S. Bartalini, S. Borri, P. Cancio, A. Castrillo, I. Galli, G. Giusfredi, D. Mazzotti, L. Gianfrani, and P. De Natale, Observing the Intrinsic Linewidth of a Quantum-Cascade Laser: Beyond the Schawlow-Townes Limit, Phys. Rev. Lett. **104**, 083904 (2010).

[19] F. Cappelli, G. Villares, S. Riedi, and J. Faist, Intrinsic linewidth of quantum cascade laser frequency combs, Optica **2**, 836 (2015).

[20] J. B. Khurgin, Y. Dikmelik, A. Hugi, and J. Faist, Coherent frequency combs produced by self frequency modulation in quantum cascade lasers, Appl. Phys. Lett. **104**, 081118 (2014).

[21] P. Friedli, H. Sigg, B. Hinkov, A. Hugi, S. Riedi, M. Beck, and J. Faist, Four-wave mixing in a quantum cascade laser amplifier, Appl. Phys. Lett. **102**, 222104 (2013).

[22] E. R. Brown, K. A. McIntosh, K. B. Nichols, and C. L. Dennis, Photomixing up to 3.8 THz in lowtemperaturegrown GaAs, Appl. Phys. Lett. **66**, 285 (1995).

[23] M. Hoffmann, J. Hebling, H. Hwang, K. Yeh, and K. Nelson, Impact ionization in InSb probed by terahertz pumpterahertz probe spectroscopy, Phys. Rev. B **79**, 161201 (2009).

[24] O. Schubert, M. Hohenleutner, F. Langer, B. Urbanek, C. Lange, U. Huttner, D. Golde, T. Meier, M. Kira, S. Koch and R. Huber, Sub-cycle control of terahertz high-harmonic generation by dynamical Bloch oscillations, Nat. Photonics **8**, 119 (2014).

[25] J. Faist, *Quantum Cascade Lasers*, 1st ed. (Oxford University Press, Oxford, 2013).

[26] G. Villares and J. Faist, Quantum cascade laser combs: effects of modulation and dispersion, Opt. Express **23**, 1651 (2015).

[27] D. Bachmann, M. Rösch, M. J. Süess, M. Beck, K. Unterrainer, J. Darmo, J. Faist, and G. Scalari, Short pulse generation and mode control of broadband terahertz quantum cascade lasers, Optica **3**, 1087 (2016).

[28] F. Wang, K. Maussang, S. Moumdji, R. Colombelli, J. R. Freeman, I. Kundu, L. Li, E. H. Linfield, A. G. Davies, J. Mangeney, J. Tignon, and S. S. Dhillon, Generating ultrafast pulses of light from quantum cascade lasers, Optica **2**, 944 (2015).

[29] A. Soibel, F. Capasso, C. Gmachl, M. Peabody, A. Sergent, R. Paiella, H. Hwang, D. Sivco, A. Cho, H. Liu, C. Jirauschek, and

F. Kartner, Active mode locking of broadband quantum cascade lasers, IEEE J. Quantum Electron. **40**, 844 (2004).

[30] S. Barbieri, M. Ravaro, P. Gellie, G. Santarelli, C. Manquest, C. Sirtori, S. P. Khanna, E. H. Linfield, and A. G. Davies, Coherent sampling of active mode-locked terahertz quantum cascade lasers and frequency synthesis (vol 5, pg 306, 2011), Nat. Photonics **5**, 378 (2011).

[31] J. Kröll, S. S. Dhillon, X. Marcadet, M. Calligaro, C. Sirtori, and K. Unterrainer, Phase-resolved measurements of stimulated emission in a laser, Nature **449**, 698 (2007).

[32] D. Oustinov, N. Jukam, R. Rungsawang, J. Mado, S. Barbieri, P. Filloux, C. Sirtori, X. Marcadet, J. Tignon, and S. Dhillon, Phase seeding of a terahertz quantum cascade laser, Nat. Commun. **1**, 1 (2010).

[33] D. Burghoff, Y. Yang, D. J. Hayton, J.-R. Gao, J. L. Reno, and Q. Hu, Evaluating the coherence and time-domain profile of quantum cascade laser frequency combs, Opt. Express **23**, 1190 (2015).

[34] J. A. Armstrong, Measurement of picosecond laser pulse widths, Appl. Phys. Lett. **10**, 16 (1967).

[35] T. Hirayama and M. Sheik-Bahae, Real-time chirp diagnostic for ultrashort laser pulses, Opt. Lett. **27**, 860 (2002).

[36] I.-C. Benea-Chelmus, C. Bonzon, C. Maissen, G. Scalari, M. Beck, and J. Faist, Subcycle measurement of intensity correlations in the terahertz frequency range, Phys. Rev. A **93**, 043812 (2016).

[37] H. Choi, L. Diehl, Z.-K. Wu, M. Giovannini, J. Faist, F. Capasso, and T. B. Norris, Gain Recovery Dynamics and Photon-Driven Transport in Quantum Cascade Lasers, Phys. Rev. Lett. **100**, 167401 (2008).

[38] T. S. Mansuripur, C. Vernet, P. Chevalier, G. Aoust, B. Schwarz, F. Xie, C. Caneau, K. Lascola, C. Zah, D. Caffey, T. Day, L. Missaggia, M. Connors, C. Wang, A. Belyanin, and F. Capasso, Single-mode instability in standing-wave lasers: The quantum cascade laser as a self-pumped parametric oscillator, Phys. Rev. A **94**, 063807 (2016).

[39] J. K. M. Vetterli and V. K. Goyal, *Foundations of Signal Processing* (Cambridge University Press, Cambridge, 2014).

[40] I.-C. Benea-Chelmus, C. Bonzon, C. Maissen, G. Scalari, M. Beck, and J. Faist, Measuring intensity correlations of a THz quantum cascade laser around its threshold at sub-cycle timescales, *Proceedings SPIE 9747, Terahertz, RF, Millimeter, and Submillimeter-Wave Technology and Applications IX* (SPIE, Bellingham, WA, 2016), p. 974715.